ARTICLE

Effect of Particle Hardness on the Penetration Behavior of Fabrics Intercalated with Dry Particles and Concentrated Particle−Fluid Suspensions

Dennis P. Kalman,[†] Richard L. Merrill,[‡] Norman J. Wagner,[†] and Eric D. Wetzel*[,‡]

Department of Chemical Engineering and Center for Composite Materials, University of Delaware, Newark, Delaware 19716, and U.S. Army Research Laboratory, Materials Division, Aberdeen Proving Ground, Maryland 21005

ABSTRACT The penetration behavior of Kevlar fabric intercalated with dry particles and shear thickening fluids (STF), highly concentrated fluid−particle suspensions, is presented. In particular, the role of particle hardness is explored by comparing fabric treatments containing SiO_2 particles, which are significantly harder than Kevlar, to treatments containing softer poly(methyl methacrylate) (PMMA) particles. The fabric testing includes yarn pull-out, quasi-static spike puncture, and ballistic penetration resistance, performed on single fabric layers. It was found that both dry particle and STF treatments resulted in improvements in fabric properties relative to neat or poly(ethylene glycol) (PEG) treated fabrics. On comparison of treatments with different particle hardness, the SiO_2 materials performed better in all tests than comparable PMMA materials, although the SiO_2 treatments caused yarn failure in pull-out testing, reducing the total pull-out energy. In addition, resistance to yarn pull-out was found to be substantially higher for STF-treated fabrics than for dry particle treated fabrics. However, both dry particle addition and STF treatments exhibited comparable enhancements in puncture and ballistic resistance. These observations suggest that viscous stress transfer, friction, and physical entrainment of hard particles into filaments contribute to the demonstrated improvements in the properties of protective fabrics treated with shear thickening fluids.

KEYWORDS: Kevlar • ballistic • shear-thickening • spike puncture • yarn pull-out • nanoparticles

INTRODUCTION

Concentrated suspensions show widely varying rheological properties, including yielding, shear thinning, and shear thickening (1−4). Shear thickening has been observed in industrial processing of concentrated suspensions, exhibiting orders-of-magnitude changes in viscosity with only slight changes in the flow kinematics (1, 2). This shear thickening behavior can lead to sudden increases in flow resistance that can damage processing equipment and hinder materials processing.

More recently, shear thickening fluids (STF) have been used in combination with protective fabrics to improve their ballistic, stab, and puncture protective properties (5−8). In general, it has been found that the addition of STF limits the mobility of yarns and filaments in the fabric, increasing the resistance of the fabric to damage mechanisms such as yarn pull-out and windowing. These observed behaviors suggest that fabric products such as body armor, protective safety-wear, inflatables, and architectural fabrics could be made more robust through the incorporation of STF−fabrics.

In spite of the breadth of experimental studies on the behavior of STF−fabrics, the existing literature provides only limited insight into the detailed mechanisms by which the STF and fabric interact to produce globally beneficial properties. Comparisons of fabrics treated with particle-free Newtonian fluids showed little correlation between fluid viscosity and ballistic behavior (7). For silica-based STFs added to aramid-based fabrics, the hard silica particles gouge and erode the surface of the softer aramid filaments in the vicinity of high applied stresses (9). This observed physical entrainment of particles could indicate that particle hardness relative to the supporting fabric plays an important role in load transfer and fabric behavior. Other studies have shown that adding dry particles to fabrics results in improvements in performance similar to those observed for STF addition (8, 10, 11). In addition, Bazhenov found that wetting Kevlar fabric with water lowered the friction, resulting in both lower pull-out resistance and lower ballistic performance (12). Lee and co-workers performed a detailed experimental and numerical study on dry fabrics and fabric−resin composites which provides insight into the complex relationship between ballistic resistance, yarn mobility, and yarn breakage (13). These results suggest that particle−fabric interactions could play a significant role in the observed properties of STF−fabrics.

Further insights into the ballistic resistance behavior of woven fabrics can be derived from numerical studies

* To whom correspondence should be addressed. E-mail: ewetzel@arl.army.mil.

Received for review August 4, 2009 and accepted October 15, 2009

[†] University of Delaware.

[‡] U.S. Army Research Laboratory.

DOI: 10.1021/am900516w

Published on Web 11/03/2009

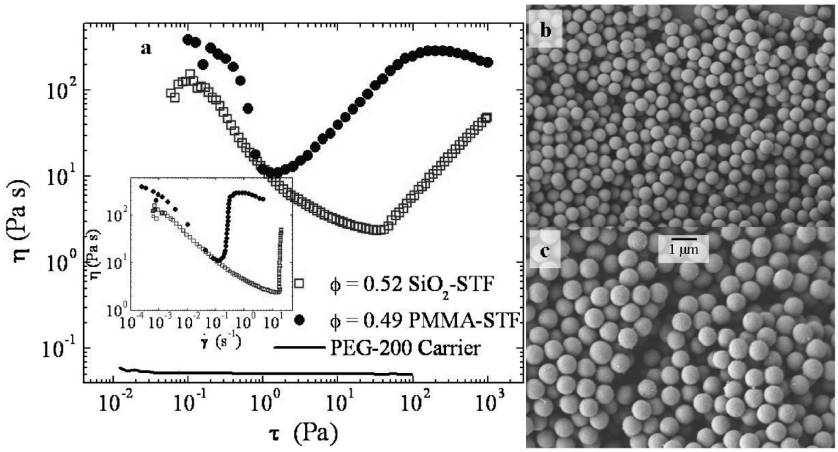

FIGURE 1. (a) Steady shear rheology of shear-thickening suspensions used and SEM micrographs of (b) commercial SiO_2 particles and (c) lab-produced PMMA particles.

(14−18). In particular, frictional effects have been studied systematically by simulations. One study on the effects of interyarn friction showed failure primarily due to windowing and yarn pull-out at very low friction, maximum performance at moderate levels of friction due to the suppression of windowing, and reduced performance at high friction due to the loss of yarn pull-out as a failure mechanism (18). Further studies showed that interyarn friction strongly influences the penetration resistance of woven fabrics by spreading the load to additional yarns not directly impacted by the projectile (14−16).

In this study, the detailed mechanisms of STF−fabric interaction are investigated through a systematic study of the effect of particle hardness and carrier fluid addition. Untreated aramid fabrics are compared to fabrics treated with a control fluid, dry particles, or shear thickening fluid−particle suspensions. Both silica and poly(methyl methacrylate) (PMMA) particles are studied, to isolate particle entrainment effects and study the effect of particle hardness. To explore a range of fabric damage mechanisms, the fabric characterization experiments include yarn pull-out (19−22), quasistatic puncture, and ballistic penetration experiments (5).

EXPERIMENTAL SECTION

Materials. Silica particles used in this study were commercially sourced, relatively monodisperse, and nominally 500 nm in diameter, and their particle and suspension properties have been characterized extensively elsewhere (23). Their density was measured by solution densitometry as 1.96 g/cm^3, and the particle diameter in poly(ethylene glycol) (PEG) was measured by ultra-small-angle neutron scattering to be 520 nm with 10% polydispersity and confirmed by SEM and DLS. The carrier fluid for SiO_2-STF and PMMA-STF was PEG (200 M_w PEG from Clariant, $\rho = 1.12$ g/cm^3, $\eta = 0.049$ Pa s), which was also used for the fluid-treated PEG−Kevlar control sample. Fluid−particle STF dispersions for rheological testing were formulated by adding the particles to PEG and roll-mixing overnight prior to testing. The steady shear rheology is shown in Figure 1 as viscosity versus applied stress, and key features are summarized in Table 1. At a particle volume fraction of $\phi = 0.52$, the STF sample exhibits extreme shear thickening, which is manifested as a nearly vertical viscosity versus rate curve at high shear rates (inset). The Newtonian rheology of the PEG is shown for reference in Figure 1.

Table 1. Tabulated Rheological Parameters for Suspensions Used

	particle type	
	SiO_2	PMMA
particle volume fraction (ϕ)	0.52	0.49
particle weight fraction	0.64	0.51
critical shear stress for shear thickening (Pa)	33.5	0.794
critical viscosity at onset of shear thickening (Pa s)	2.34	11.0
critical shear rate for shear thickening (s^{-1})	14.4	0.115

PMMA particles were chosen for this study due to their ease of synthesis, compatibility with PEG-based STF processing, and expected lower hardness relative to SiO_2. The PMMA particles were synthesized via a free-radical reaction of dilute methyl methacrylate monomer in mixed methanol and water solvent at 70 °C for 3 h (24). To make sufficient PMMA particles for this study, two separate batches of approximately 1.5 L total volume were used; the procedures for each were the same, and the effective size determined from dynamic light scattering (DLS) was not significantly different. The reaction materials were dialyzed against three separate batches of deionized water for at least 24 h each and then concentrated via centrifugation to 31.5 wt % solids before intercalation into fabric as discussed below or transfer into PEG for rheology measurements. To produce a suspension for rheology measurements, sufficient PEG-200 was added to achieve an STF volume fraction of $\phi = 0.496$ (volume of PMMA normalized by total volume of PMMA and PEG), and then the water was removed by first heating while stirring at 60 °C and then under vacuum at 60 °C. This formulation of PEG−PMMA has been shown to exhibit shear thickening behavior, and its rheology is also seen in Figure 1 (25). The particles produced had a density of 1.23 g/cm^3 determined by solution densitometry in water by standard procedures assuming ideal mixing (26) and a diameter of 1050 ± 110 nm determined via DLS and confirmed via SEM. SEM micrographs of both particle types are also shown in Figure 1.

For in-fabric testing, the particles and/or carrier fluid were intercalated into sheets of JPS Composites (Anderson, SC) scoured Style 706 woven Kevlar fabric (600 denier KM2 yarns, plain-woven at 34 × 34 yarns per inch), with an areal density of 180 g/m^2. In each case, the appropriate materials were diluted with ethanol, and individual fabric sheets were dipped and held in the solution for at least 1 min before being squeezed through rubber-coated nip rollers and hung to dry at room temperature. After air-drying for at least 10 min, the fabric was

Table 2. Data of Fabric Treatment Add-on and Test Results

	neat	PEG	PMMA-dry	PMMA−STF	SiO_2-dry	SiO_2−STF
Fabric Data						
areal density (gsm)	180	192 ± 0.85	189 ± 2.07	196 ± 1.49	193 ± 1.51	205 ± 1.26
weight addition (%)		6.55 ± 0.47	4.97 ± 1.2	9.16 ± 0.83	7.12 ± 0.84	14.0 ± 0.72
total volume addition (%)		8.42 ± 0.61	5.82 ± 1.4	11.2 ± 1.0	5.48 ± 0.64	13.3 ± 0.69
particle volume addition (%)			5.82 ± 1.4	5.58 ± 0.51	5.48 ± 0.64	6.92 ± 0.36
fluid volume addition (%)		8.42 ± 0.61		4.09 ± 1.6		4.09 ± 1.9
Yarn Pull-Out Data						
loading peak force (N)	13.0 ± 0.27	20.4 ± 0.73	25.3 ± 1.9	46.7 ± 2.9	37.2 ± 1.2	61.8 ± 7.2
loading displacement (mm)	8.56 ± 0.75	9.87 ± 0.65	12.0 ± 1.3	18.6 ± 2.5	16.5 ± 1.5	24.0 ± 2.2
plateau force (N)	8.40 ± 1.3	20.1 ± 1.3	13.9 ± 2.9	30.4 ± 3.1	32.4 ± 2.0	N/A
plateau location (mm)	8−60	19−64	12−60	21−66	16−62	N/A
total energy (J)	0.609 ± 0.022	1.44 ± 0.056	1.00 ± 0.075	2.31 ± 0.093	1.81 ± 0.036	1.04 ± 0.27
Spike Puncture Data						
peak force (N)	21.7 ± 3.5	31.7 ± 9.1	36.3 ± 6.5	58.1 ± 13	77.6 ± 9.7	70.4 ± 15
failure distance (mm)	8.19 ± 0.43	7.83 ± 0.84	8.99 ± 0.48	9.71 ± 0.46	10.3 ± 0.63	10.3 ± 1.1
failure energy (J)	50.0 ± 11	71.1 ± 28	91.4 ± 24	163 ± 48	215 ± 43	193 ± 49
Ballistic Data						
ballistic V_{50} (m/s)	72.2 ± 6.9	77.4 ± 4.0	138 ± 4.8	136 ± 5.0	217 ± 6.6	196 ± 4.5

dried in an oven at 60 °C for 30 min to remove the ethanol and/or water co-solvents. The resulting fabrics were dry to the touch, even for the PEG, SiO_2−STF, and PMMA−STF materials which include PEG carrier fluid. Fabrics with PEG carrier had a uniform appearance, while PMMA- and SiO_2-coated fabrics without PEG appeared streaky with a whitened or slightly chalky appearance. If placed in contact with surfaces such as benchtops or gloved hands, fabrics treated with the dried particle addition left a white residue of dry particles on the surface. In contrast, coated fabrics with PEG and particle STF suspension addition left no obvious residue on contact surfaces.

The mass or volume addition of each coating to the fabric can be controlled by tailoring the dilution ratio of coating to co-solvent in the dip bath. For the present study, we wish to compare coatings utilizing SiO_2 and PMMA particles, with and without PEG carrier fluid. A comparative series of coated fabrics could be formulated to maintain a consistent coating mass, coating volume, particle mass, or particle volume. We have chosen to design our fabric set to compare fabrics with consistent particle volume addition. This selection is based on previous observations that submicrometer particles intercalate between fibers and yarns in the void space of the woven fabric (6, 10, 27, 28), so that a consistent particle volume addition should result in reasonably consistent geometric packing and fill of the particles in the coated fabrics. This geometric consistency allows for the most objective comparison of the effect of particle hardness and solvent addition on overall fabric performance. Other comparisons, such as constant coating weight, could be more relevant to practical protective material design and would be valuable for additional study.

Six different fabric coatings, seen in Table 2, were compared: untreated (neat), liquid control (PEG), dry PMMA (PMMA-dry), PMMA with PEG (PMMA-STF), dry SiO_2 (SiO_2-dry), and SiO_2 with PEG (SiO_2-STF). To achieve constant particle addition to the fabrics, dip baths for each particle-based coating were designed to a consistent ratio of total particle volume to co-solvent volume. This ratio ended up being 0.163 for the PMMA treatments and 0.173 for the SiO_2 treatments (the error resulted from a slight change in the PMMA particle density from the expected value from previous work). For the dry PMMA coating dip bath, ethanol was added to the concentrated particles in water (31.5 wt % solids) to achieve the desired particle to co-solvent volume ratio. For the PMMA−STF coating dip bath, an identical PMMA−water−ethanol dip bath was modified by adding sufficient PEG-200 to achieve an STF volume fraction of $\phi = 0.496$. For the dry SiO_2 coating dip bath, ethanol was added directly to the SiO_2 particles to achieve the desired particle to co-solvent volume ratio of 0.173. For the SiO_2−STF coating dip bath, an identical SiO_2−ethanol dip bath was modified by adding sufficient PEG-200 to achieve an STF volume fraction of $\phi = 0.52$. The PEG fabric (no particles) was produced using a bath with the same volume ratio of PEG to ethanol (0.217) as in the SiO_2-STF bath. For each case, the coating mass and volume additions as a percent add-on of the mass or volume of the fabric are summarized in Table 2.

For each coating, two sheets of 38.1 cm × 38.1 cm fabric were produced for ballistic testing (later cut into 15.2 cm × 5.08 cm strips), one sheet of 25.4 cm × 20.3 cm fabric was produced for pull-out testing, and one sheet of 15.2 cm × 15.2 cm fabric, cut on a 45° bias, was produced for puncture testing (cut into two 15.2 cm × 7.62 cm pieces).

Methods. Yarn pull-out testing was performed using a 20.3 cm × 20.3 cm sheet of fabric with transverse yarns removed on the top and bottom to create free lead and tail yarns, respectively (parts a and b of Figure 2). The fabric was put in a frame with two clamped edges (0.635 cm in each clamp, leaving 19.1 cm of fabric between the grips) at a transverse tension of 100 N, with 10.2 cm of lead yarn and a 5.08 cm tail. The lead yarn was clamped in a pneumatic grip mounted in an MTS Synergie load frame and pulled at a rate of 50 mm/min until the yarn was completely removed or completely broken. To account for slack, zero displacement was defined as the displacement at which the force first reaches 0.1 N. For further details, see Kirkwood et al. (20). Note that the fabric elastically deforms slightly upward as the yarn is being pulled (Figure 2b), so that the crosshead displacement is slightly larger than the true yarn displacement relative to the fabric during most of the experiment (20).

Yarn pull-out testing consists of three distinct stages (20). In the first stage, uncrimping, the yarn is progressively straightened from the top to the bottom of the fabric. During this stage the load on the yarn rises rapidly, reaching a peak value when

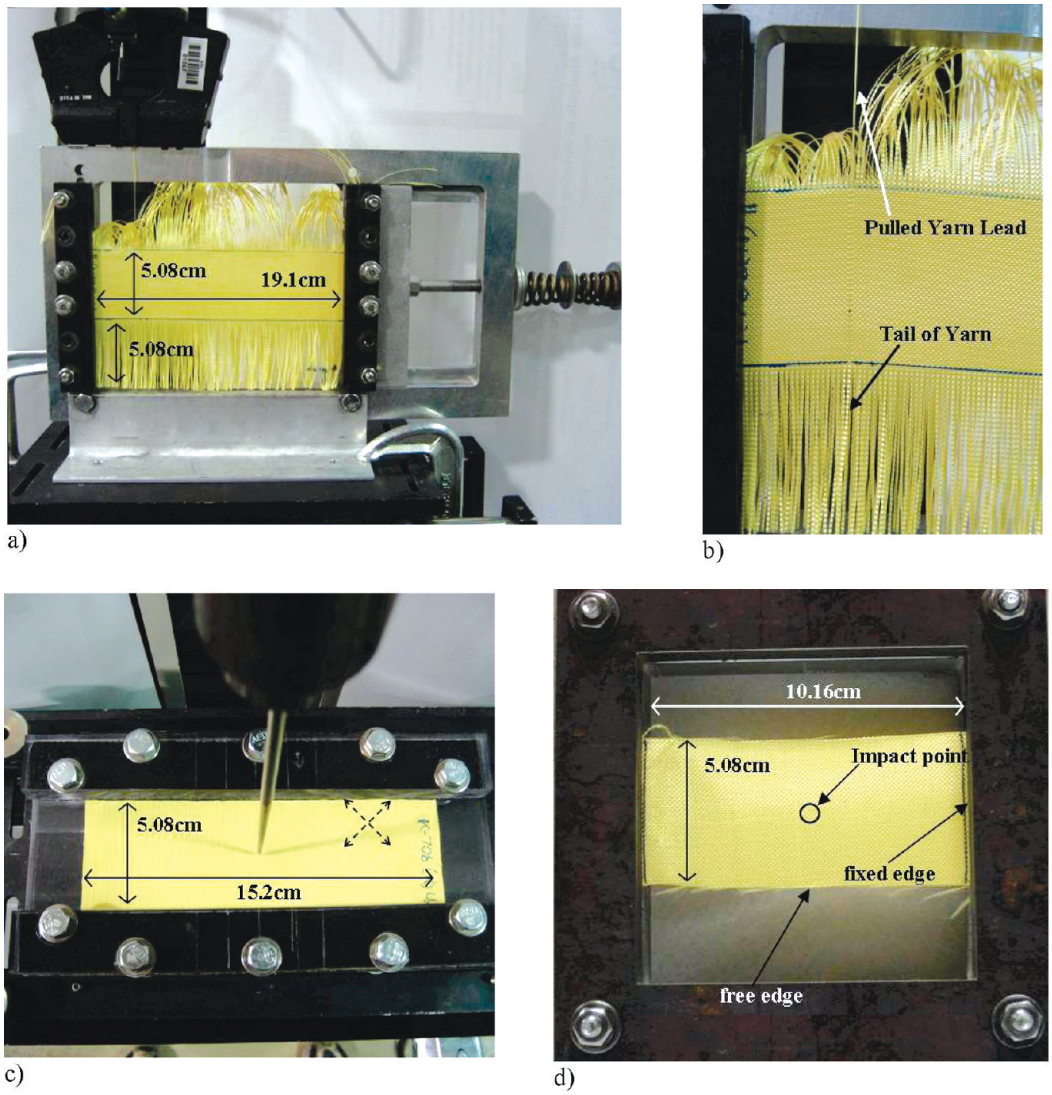

FIGURE 2. (a) Yarn pull-out testing apparatus. (b) Closeup of pulled yarns in yarn pull-out testing. (c) Spike puncture testing apparatus. Dashed arrows indicate fabric weave orientation. (d) Ballistic V_{50} testing frame.

the yarn straightening has progressed past the final, bottom transverse yarn. The load then typically drops slightly, as static friction is overcome and the yarn begins to translate through the fabric. During this second stage, which is referred to as the plateau region, the load exhibits oscillating behavior, typically around a constant average pull force, as the residual crimp in the yarn moves alternately over and under transverse yarns. The length of this average load plateau is approximately equal to the length of the original yarn tail. As the end of the yarn tail reaches the lowest transverse yarn and begins to pull through the fabric, the yarn load drops monotonically as fewer and fewer transverse yarns are engaged. This third stage of pull-out continues until the yarn is fully extracted from the fabric and the pull force drops to zero. In some cases, the yarn breaks rather than completely pulling out, and only the first stage and sometimes part of the second stage are observed.

The yarn pull-out data are summarized as loading peak force (the peak force at the end of the first, uncrimping stage), loading displacement (location of the loading peak force), and plateau force (average force during the second, constant yarn translation stage). The total, integrated energy for yarn pull-out is also tabulated, although it does not provide a consistent measure of resistance to pull-out since some materials exhibit yarn breakage rather than pull-out. Also included for completion is the crosshead displacement range of the force plateau.

The quasi-static puncture testing used a single 15.2 cm × 7.62 cm fabric strip, cut on a bias so that the yarns are oriented at 45° relative to the edges of the strip. This bias configuration allows multiple, consistent puncture experiments to be executed on a single strip of fabric without significant interaction between puncture events, as unique principal yarns are engaged in each puncture. The fabric strip was mounted in a frame as seen in Figure 2c with 1.27 cm of fabric clamped along the long edges of the fabric, with the shorter edges of the fabric unclamped, such that a 15.2 cm × 5.08 cm unbacked fabric strip is exposed. An MTS Synergie load frame was used to push a National Institute of Justice standard spike (29) from Industrial Knife and Cutter (Simpsonville, SC) into the fabric at a rate of 5 mm/min. Five penetration measurements were performed on each fabric strip, spaced evenly along the center line of the strip. Zero displacement was again defined as the displacement at which force is equal to 0.1 N. The NIJ spike has an initial, relatively sharp tip angle along its first 4 mm, followed by a less acute, more gradual but increasing shaft angle over its remaining length. This spike geometry results in a loading curve that shows gradual initial loading as the spike begins to push against the fabric, including one or more dips in the curve due to partial tip breakthrough, followed by a sharp drop when the spike tip penetrates completely through the fabric, and finally a long tail of low but slightly increasing force as the fabric is pushed

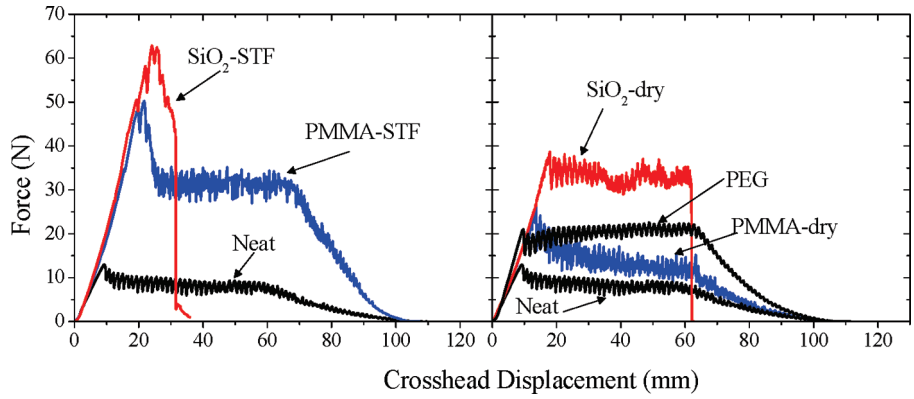

FIGURE 3. Typical force versus crosshead displacement curves from yarn pull-out testing for various fabric treatments.

through the gradually increasing diameter of the main shaft. The puncture data are summarized as peak force (which may not be at the final breakthrough point if a partial tip breakthrough point occurs near the final breakthrough), displacement at failure, and integrated energy to failure, which does not include the final tail region after the spike tip has broken through the fabric.

Ballistic testing is performed by firing spherical steel projectiles of 0.22 caliber (5.56 mm diameter) and 0.692 ± 0.002 g from a smooth-bore helium gas gun at single-layer fabrics. The velocity is adjusted by varying the gas pressure and measured by a time-of-flight light chronograph in front of the target. As seen in Figure 2d, the fabric is clamped along two edges in a steel frame with adhesive grip tape on contact surfaces to increase frictional coupling. The fabric strips used are 15.2 cm × 5.08 cm, with 2.54 cm clamped along each fixed edge, leaving a 10.2 cm × 5.08 cm exposed area. The fabric yarns are oriented orthogonally relative to the edges of the clamping frame. A thin plastic bag is taped on the back of the target frame to act as a witness (5). If the projectile is in the bag or penetrates through the bag after impact, it is considered a penetrating impact. Ballistic performance was characterized by impacting the targets at a range of velocities, until a data set was achieved with five penetrating impacts and five nonpenetrating impacts in which all impact velocities were within 7.62 m/s (25 fps) of the average of those ten impact velocities. The average velocity of these five penetrating and five nonpenetrating impacts is reported as the V_{50}, the velocity at which the projectile is expected to exhibit a 50% probability of penetration (30).

RESULTS

Yarn Pull-Out Testing. Typical curves of force versus crosshead displacement for each material are shown in Figure 3. In the neat, PEG, PMMA-dry, and PMMA-STF cases, the yarn uncrimps in a loading regime, shows a force plateau where the yarn pulls through the fabric weave, and then shows a steady force decay as the fiber pulls out of the weave. The peak force is generally noted at the end of the loading regime, but in the PEG-fabric the load increases slightly through the "plateau" region. In addition, the PMMA-STF fabric shows unique behavior of a significant drop (~30%) in load from the peak to the plateau. The extracted yarns appear to be in good condition, with little evidence of significant damage or fraying. In the SiO_2-dry case, the yarn tail is pulled partially through the weave (seen by the force plateau after fiber uncrimping) but generally breaks before the end of the tail enters the woven fabric. During pull-out for SiO_2-dry samples, the yarn becomes very frayed, and

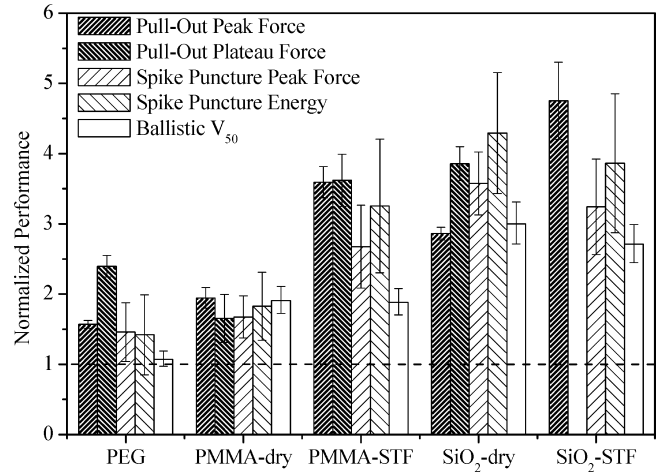

FIGURE 4. Summarized test data. Reported values are normalized by the corresponding value for the neat fabric. For yarn pull-out and spike puncture test results, error bars indicate one standard deviation above and below the average of five measurements, normalized by the neat value of that measurement. No pull-out plateau force is reported for the SiO_2-STF case, due to yarn breakage. For ballistic V_{50} measurements, error bars indicate the range of data values used to calculate V_{50}, normalized by the neat fabric V_{50} value.

yarn fracture typically occurs on the pulled yarn at a position along its length that is still embedded inside the woven fabric. For SiO_2-STF fabrics, the yarn becomes very frayed and "fuzzy" during the uncrimping stage, but in most cases uncrimping appears to progress completely through the fabric. Yarn fracture typically occurs after little or no yarn translation has occurred, with the fracture point again located on the pulled yarn at a location within the woven fabric. It is also interesting to note that ink marks on the pulled yarn appeared to "smear" as the yarn was pulled, indicating that individual filaments were being pulled at different rates. This observation implies that yarn failure is occurring gradually at a filament-by-filament progression.

Summarized data from yarn pull-out testing are shown in Table 2, including loading peak force, loading displacement, plateau force, location of the plateau, and total integrated failure energy. Additionally, Figure 4 shows the value of loading peak force and plateau force for the various treatments relative to the value in the neat case. All treated materials require forces to load and pull out the yarn higher than that for the neat material. In addition, the STF-treated fabrics require significantly higher forces than the respective

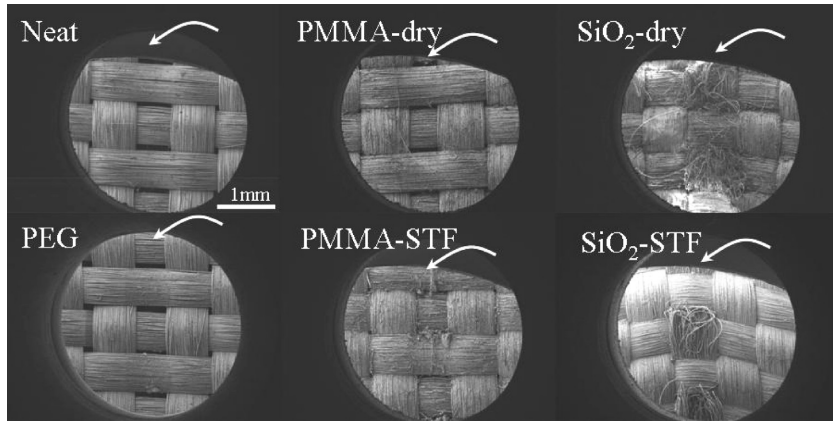

FIGURE 5. SEM micrographs of fabric from pull-out testing. The arrow indicates the former position of the extracted yarn, or in the SiO_2 cases, the fractured, pulled yarn.

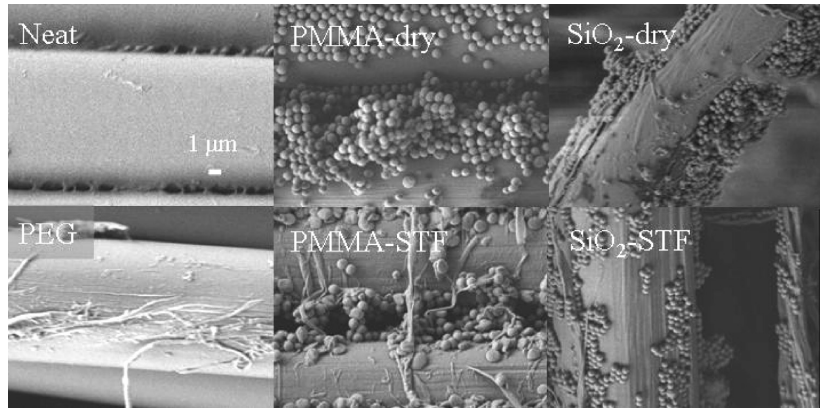

FIGURE 6. SEM micrographs of fabric from pull-out testing. The PMMA and particle-free fabrics show filaments of cross yarns, whereas SiO_2 fabrics show filaments from the pulled yarn.

dry particle treated fabrics. The loading forces for the PMMA-treated fabrics are also lower than the comparable SiO_2-treated fabrics. Note, however, that the PMMA-STF fabric, which showed no obvious fraying during pull-out, has a higher peak force than the SiO_2-dry fabric, which exhibited yarn breakage during pull-out. The PEG fabric has a slightly lower loading force than the PMMA-dry fabric but a higher plateau force. This suggests that the liquid itself increases both the static friction (adhesion between yarns) and increases the dynamic friction, possibly due to viscous dissipation in the fabric.

SEM micrographs at low magnification for the fabrics after yarn pull-out can be seen in Figure 5. These images are oriented so that the direction of pull is upward, with the original extracted yarn position located at the center of the image. The yarns were fully extracted in the neat, PEG, and PMMA fabrics but not for the SiO_2 fabrics, where a significant fraction of the original pulled yarn filaments remain in the fabric. Figure 6 shows a higher magnification micrograph of either the cross-yarn exposed by removal of a vertical yarn or the yarn which was pulled in the SiO_2 cases. Areas of significant fiber scoring on large fractions of the yarn surface by the SiO_2 particles can be seen, but only limited fiber scoring is seen in the PMMA cases. Another key difference is that the SiO_2 particles all appear to be very spherical in shape, while many of the PMMA particles appear to have been flattened. This flattening of PMMA particles was not observed for virgin PMMA-treated fabrics and therefore appears to be the direct result of the yarn pull-out process. The neat, PEG, and PMMA fabric weaves appear to have recovered to an orthogonal orientation after the pull-out experiment, whereas the high force on the SiO_2-STF fabric combined with the limited mobility has deformed the weave irreversibly such that the cross yarns have been displaced in the direction of yarn pull-out.

Puncture Testing. Typical curves of force versus displacement for the spike puncture testing for each material are shown in Figure 7. Table 2 summarizes the data in terms of peak force, displacement at failure, and integrated failure energy. Figure 4 also shows the relative value of peak force and failure energy of the treated fabrics to the neat fabric. Much of the variability seen in puncture testing is due to the woven nature of the fabric. The lowest penetration forces for a particular specimen were observed when the spike initially contacted an interstitial position between yarns, leading to penetration primarily due to fabric "windowing" (9) (also referred to as "wedge through" (31)). Windowing refers to the spreading apart of yarns in a woven fabric, creating an open area through which an object can penetrate. In contrast, the highest penetration forces occurred when the spike first contacted the fabric at a yarn crossover

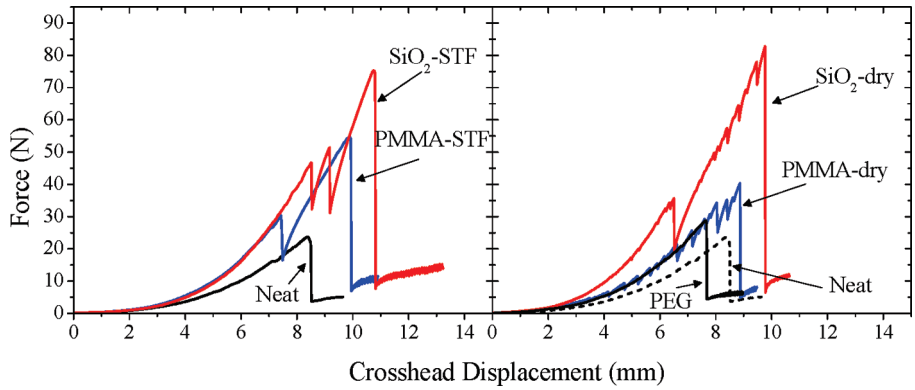

FIGURE 7. Typical force versus crosshead displacement curves for quasi-static spike puncture testing for various fabric treatments.

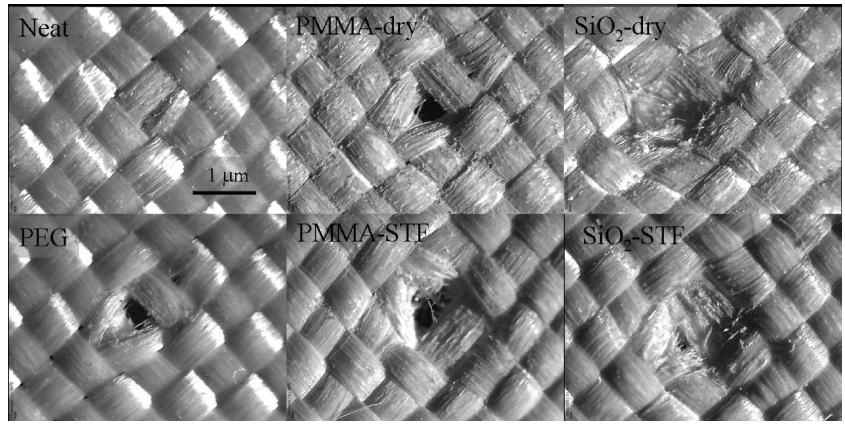

FIGURE 8. Optical micrographs of fabric from spike puncture testing.

area, leading to a higher likelihood of yarn pull and fiber fracture with windowing during penetration. In spite of this variability, statistically significant differences in the energy and peak force were measured between the PMMA-treated fabrics and the SiO_2-treated fabrics.

A significantly larger force, resulting in larger energy, was required to puncture the PMMA-STF fabric compared to the PMMA-dry fabric. As in the pull-out testing, the PEG fabric has similar peak force and failure energy compared to the PMMA-dry fabric. The SiO_2—STF fabric requires slightly less force to puncture than the SiO_2-dry fabric. The two SiO_2 materials have higher peak loads and failure energies than the PMMA-STF fabric. Figure 8 shows optical micrographs of the spike puncture testing. Kevlar yarns and fibrils were broken for the SiO_2-treated fabrics. In addition to fiber breakage, windowing of the fabric weave and splitting of the yarn into separate bundles of fibers both appear to be associated with fabric failure.

Ballistic V_{50} Testing. The ballistic test results are shown in Table 2, and the V_{50} values relative to that of the neat fabric are shown in Figure 4. The V_{50} values for the PMMA-dry and PMMA-STF fabric are both about 140 m/s, nearly double that of the neat and PEG fabrics. The SiO_2-dry and SiO_2-STF fabric both have V_{50} values over 195 m/s, about triple that of the neat fabric and about 50% higher than for the PMMA fabrics. No significant difference is seen in the V_{50} between the PMMA fabrics, although the SiO_2-dry fabric appears to show a slightly higher V_{50} than the SiO_2-STF fabric. Since the failure energy is related to the velocity squared, the SiO_2 fabrics have about 1 order of magnitude higher failure energy than the neat fabric. In Figure 9, which shows pictures of the failed fabrics, windowing is seen with local yarn uncrimping and limited yarn extraction in the neat case. In the PEG and PMMA materials, significant yarn uncrimping and extraction is evident (via ~2—3 cm long yarn loops pulled out at the damage zone). In addition, no yarn breakage is seen in the neat, PEG, or PMMA materials. In the SiO_2 materials, significant uncrimping is evident with very little yarn extraction, and the extracted fiber loops are much smaller (<0.5 cm). In addition, significant fiber breakage is seen for the SiO_2 materials. In the neat materials, yarn uncrimping and extraction does not appear to be significantly biased directionally; however, the PMMA and SiO_2 materials show only a limited damage zone in the horizontal direction but show uncrimping and fabric deformation over broader areas in the vertical direction. This bias in yarn uncrimping is consistent with the fixed boundaries in the horizontal direction limiting yarn pull-out and the free edges allowing pull-out in the vertical direction. The SiO_2 materials also show some tearing of the fabric weave at the fixed edge, far away from the impact point, which is not seen for the neat, PEG, or PMMA materials.

DISCUSSION

The experiments performed in this study—yarn pull-out, quasi-static puncture, and ballistic penetration—explore a

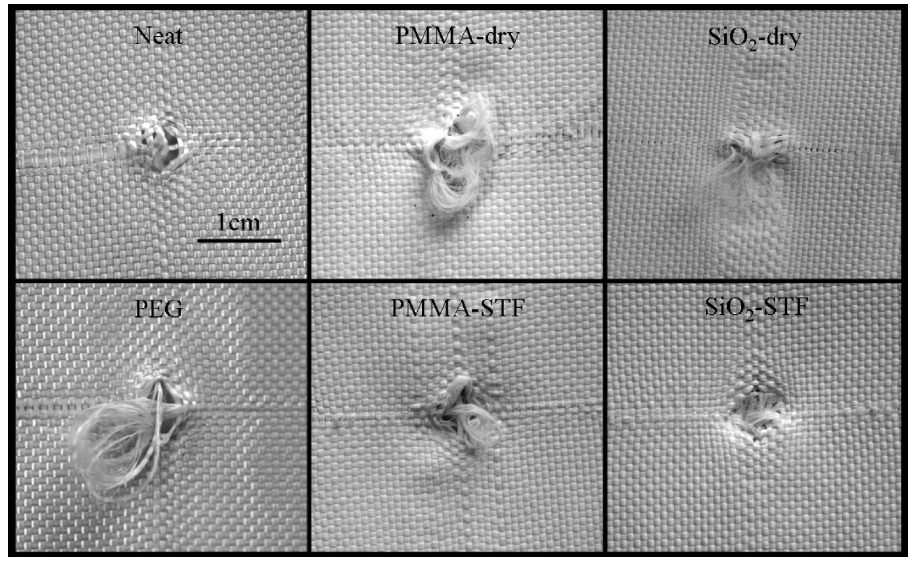

FIGURE 9. Front faces of fabric after ballistic testing. Yarn pull-out and windowing are seen in the neat (left) and PMMA (center) fabrics, with fiber breakage and limited pull-out seen in the SiO_2 fabrics (right).

range of fabric defeat mechanisms including yarn uncrimping, yarn sliding and extraction, windowing, yarn and fiber compression, and fiber shear and tensile failure. These mechanisms can be broadly characterized as being dependent on either mechanical properties inherent to the yarn filaments or the effects of mobility of the yarn or filament. For example, yarn sliding and windowing are most directly modified by restricting the ability of fibers and yarns to reorganize and move relative to each other. In contrast, compression, shear, and transverse failure are more directly related to the mechanical properties of the Kevlar filaments.

The results of this study show that intercalation of particles into fabrics, whether dry or wetted, overall leads to a substantial increase in fabric resistance to yarn pull-out, puncture, and ballistic penetration. It is unlikely that the intercalation of particles increases the inherent mechanical properties of the Kevlar filaments, as the particles are located primarily outside of the filaments and therefore should not provide mechanical reinforcement to the fiber. Therefore, these modifications to fabric behavior are most likely generated due to changes in the mobility-driven defeat mechanisms.

Particle hardness is shown here to be an important factor governing the behavior of particle-intercalated fabrics. All experiments showed a systematic increase in resistance for SiO_2 systems as compared to PMMA systems. If we accept the hypothesis that mobility mechanisms are primarily engaged in these experiments, then the harder particles must be more effective at reducing yarn and filament mobility. One obvious explanation for this behavior is that the harder particles are able to embed into the softer polymer filaments, leading to more direct mechanical coupling between fibers and particles. The SEM micrographs from this and previous studies (9) indicate that this mechanism is relevant. A different explanation would be that, under stress, the softer particles are more likely to accommodate loads through direct mechanical deformation. This accommodation could lead to less resistance to bulk compression and reorganization mechanisms, resulting in reduced effect on fabric mobility. This second hypothesis is supported by the appearance of deformed PMMA particles after testing. The drop in pull-out load after the initial peak in the PMMA-STF-Kevlar, a feature unique to this treatment, could be symptomatic of these particle deformations. Further experiments are required to determine the relative importance of each of these mechanisms.

During yarn pull-out testing, yarn fracture was observed only for the treatments with SiO_2 particles. However, peak forces for the PMMA-STF pull-out case, in which complete yarn extraction was observed, are higher than the peak forces experienced by the SiO_2-dry case prior to yarn fracture. This result shows that the presence of harder particles can lead to a reduction in yarn and fiber mechanical properties under certain conditions. Direct characterization of the effect of particle intercalation on the tensile strength of yarns, although not reported in this study, could provide important insights into these mechanisms. There likely are specific fabric applications where this degradation effect due to the hard particles is detrimental, where particle hardness may need to be tuned for optimal behavior. For example, it is reasonable to postulate that there exist particles with hardness intermediate between PMMA and SiO_2 that would result in higher pull-out resistance than PMMA but would not induce premature yarn failure, as observed for SiO_2-based coatings.

We should also acknowledge that the SiO_2 and PMMA particles are not identical in size (the PMMA particles are larger by a factor of 2); thus, there could be secondary effects due to particle size that limit the universality of our conclusions with respect to particle hardness. However, prior studies by our group (6, 28) have shown that particle size plays only a minor role in fabric performance, as long as the particles are small enough to intercalate between filaments. Another recent study comparing 100−500 nm particles showed a slight change in ballistic performance with de-

creasing particle size (7). However, these observed differences do not appear to be significant enough to account for the behavioral differences we have observed between PMMA and silica systems.

The role of a fluid carrier in STF coatings, as compared to dry particle systems, is complex. In yarn pull-out testing, pure PEG addition increases both the static friction and dynamic friction as compared to those of the neat fabric. These effects lead to a moderate increase in puncture resistance but little change in ballistic performance relative to the neat fabric. The combined addition of both fluid and particles as an STF formulation, compared to dry particle treatments, leads to a dramatic increase in yarn pull-out resistance for PMMA- and SiO_2-treated fabrics and a significant improvement in puncture resistance for the PMMA-treated fabrics. However, the STF treatments lead to slight *decreases* in fabric performance relative to dry particle fabrics for both systems in ballistic testing and SiO_2 systems in puncture.

One possible explanation for these trends in behavior is that penetration behavior may not be optimized at maximum mobility restriction but at some intermediate, tuned degree of mobility. For example, for the fabric and projectile combination used in the present study, penetration is accommodated in neat fabrics by mobility mechanisms such as windowing and yarn pull-out. Therefore, higher mobility restriction is required. However, the yarn pull-out experiments show that SiO_2-STF coatings drastically restrict yarn pull-out, leading to yarn failure with little extraction. In contrast, the SiO_2-dry showed the capacity for yarn extraction during yarn pull-out at high pull force. Therefore, under ballistic impact, the yarns in this fabric may be free to pull slightly, absorbing energy, lengthening the interaction time with the projectile, and decreasing the severity of the instantaneous stresses on the yarns and filaments. Under this scenario, the very high pull-out resistance of the SiO_2-STF treatment is detrimental to overall penetration performance. This example underscores the important conclusion that a reduction in yarn mobility is not always beneficial; it is more likely that there exists an optimal degree of mobility for a given fabric and threat combination. The particle hardness, particle-to-fluid ratio, and coating-to-fabric ratio all provide means of tuning the performance of the coated fabric. This conclusion is supported by earlier numerical studies, which predicted that the ballistic resistance of a fabric would be highest at an optimal, intermediate yarn−yarn frictional value (12). At this optimal value, fabric windowing is fully repressed, but enough slippage is permitted to reduce instantaneous stress concentrations in the vicinity of the impact.

On a more fundamental level, the results show that both frictional and viscous mechanisms may be relevant in these coated fabrics. For example, the behavior of the dry systems seems best described as a "frictional" effect, since no fluid is present. However, due to the very small size of the particles relative to the filament diameter and interstitial volumes, the dry coatings are more like a granular bed than a simple frictional coating (9). Under this view, even the dry coatings will "flow" under deformation, and a simple surface friction model would be an incomplete representation of material behavior. Regarding viscous fluid effects, the yarn pull-out experiments in particular appear to show a strong effect due to the presence of the liquid carrier. It is particularly striking that the addition of PEG, without particles, leads to an increase in yarn pull-out resistance. It is not clear if this increase in resistance is due directly to viscous shear of the coating or due to some indirect effect such as reducing the ability of the yarns to compress to a cross-sectional shape that more easily accommodates yarn extraction.

While the results suggest that the rheological viscous coupling is certainly relevant, the specific role of the shear thickening rheology requires further investigation. The dramatic enhancement in yarn pull-out behavior for STF-treated fabrics relative to neat and dry particle treatments implies that the STF coatings do not simply behave as a linear combination of the constituents. Rather, the full rheological response of the STF fluids themselves must be considered. The strong shear thickening response for the STF fluids demonstrated in Figure 1 could lead to substantial load coupling between yarns and, hence, the extreme forces required for yarn pull-out. The detailed rheological response of PMMA-STF versus SiO_2-STF in Figure 1 could also be related to observed trends in their behaviors as coatings. The downward trend in measured viscosity for the PMMA case at high stresses is believed to be associated with particle deformations (25). These same particle deformations appear to also play a role in the reduced yarn pull-out force for these PMMA coatings.

One complicating factor in determining the role of STF rheology is that the extremely high surface area of the fabric could cause microscale segregation of fluid and particle phases. Since STF rheology is known to be highly sensitive to particle volume fraction, it is possible that the local composition and behavior of the coating varies relative to the original bulk STF properties. However, as noted above, the results cannot be explained by simply adding the properties of the PEG and dry particle treated samples, implying the presence of coupled physical effects. Furthermore, the physical appearance of the STF-treated fabrics shows none of the flaking and dustiness associated with the dry particle treated fabrics. These observations suggest that particles are predominantly incorporated in the form of a colloidal dispersion and, given the compositions possible, that dispersion will exhibit shear thickening.

A second challenge in predicting in situ rheological behavior is estimating stresses within the complex geometry of a woven fabric. The transitional behavior of an STF is fundamentally triggered by critical stress levels (32), rather than deformation rates, and these stresses are not limited to shearing (33, 34). For example, it is possible that compression in a highly confined geometry can lead to high local stresses that induce STF transition. We can estimate characteristic stress levels for each of our experiments to determine the likelihood of a shear-thickening response (detailed

calculations are included in the Supporting Information). For yarn pull-out, normalizing the peak pull-out force by the yarn−yarn sliding contact area for a single yarn gives a characteristic shear stress of 10^6 Pa, many orders of magnitude higher than our STF transitional stresses of ~1−100 Pa. For the puncture experiment, normalizing the typical puncture force by a representative spike tip surface area provides a compressional stress of 10^6 Pa: again, high enough to induce transition. For the ballistic experiments, the stress on the fabric can be estimated by normalizing the deceleration force by the projectile area; the estimated compressional stress value, 10^7 Pa, is also well beyond the critical transitional stresses for our STF systems. Therefore, the stresses encountered by the STFs intercalated in the small gaps between the fibers are likely to be sufficient to trigger shear thickening. Future studies could search for signatures of shear thickening behavior in STF-fabrics by conducting puncture and pull-out experiments at varying loading rates.

Note that the experiments in this study included only single-layer, unbacked fabric layers. While we expect many of these results to be broadly applicable, further testing is required to determine whether these conclusions apply to the performance of multilayer targets or unclamped targets on soft substrates.

On a practical level, and perhaps most importantly, there appears to be a major benefit to the liquid carrier in terms of handling and coating durability. The fabrics intercalated with dry particles tend to shed particles on most surfaces that they touch and even into free space if they are handled roughly. This behavior is not surprising, as there is no obvious binding force to keep the particles in contact with the fabric. In addition to dangers associated with nanoparticle emission into the environment, this shedding of particles suggests poor long-term durability of these coated fabrics. Their generally blotchy and nonuniform appearances also suggest the potential for inconsistent point-to-point behavior. In contrast, the particle-intercalated fabrics with liquid carriers look uniform and can be handled roughly and directly with little evidence of coating loss or transfer. This behavior suggests that the liquid carrier entrains the particles within the fabric through a capillary or wetting mechanism. From this practical viewpoint, the STF treatments appear to result in more durable and robust coatings, while providing puncture and pull-out performance comparable to or better than dry particle coatings. The presence of the liquid carrier also provides opportunity for incorporation of secondary functionalities, such as hydrophobicity or antimicrobial action.

CONCLUSIONS

The results of this study show that particle intercalation is an effective means to significantly modify the behavior of woven fabrics, primarily through a decrease in yarn and fiber mobility. Harder particles tend to result in a greater reduction in mobility than softer particles, as they are more likely to mechanically engage filaments and less likely to accommodate stress via particle deformation. In addition, the inclusion of a liquid carrier with the intercalated particles tends to further restrict mobility, while dramatically improving the robustness and practicality of the coating. The results also show that, for some fabric performance metrics, a tuned level of mobility may be preferable to engineering extreme levels of restricted mobility.

Acknowledgment. Research was sponsored by the U.S. Army Research Office and U.S. Army Research laboratory and was accomplished under Cooperative Agreement Number W911NF-05-2-0006. The views and conclusions contained in this document are those of the authors and should not be interpreted as representing the official policies, either expressed or implied, of the Army Research Office, Army Research Laboratory, or the U.S. Government. The U.S. Government is authorized to reproduce and distribute reprints for Government purposes, notwithstanding any copyright notation hereon. We also thank Joe Houghton for earlier work on this project.

Supporting Information Available: Calculations for the characteristic stress in the shear thickening fluid-fabric composites undergoing yarn pull out, spike puncture, and ballistic testing are included in the Supporting Information. This information is available free of charge via the Internet at http://pubs.acs.org.

REFERENCES AND NOTES

(1) Barnes, H. A. *J. Rheol.* **1989**, *2*, 329–366.
(2) Beazley, K. M. In *Rheometry: Industrial Applications*; Walters, K., Ed.; Research Studies Press: Chichester, U.K., 1980; pp 339−413.
(3) Boersma, W. H.; Laven, J.; Stein, H. N. *J. Rheol.* **1995**, *39*, 841–860.
(4) Brady, J. F. *J. Chem. Phys.* **1993**, *99*, 567–581.
(5) Decker, M. J.; Egres, R. G.; Wetzel, E. D.; Wagner, N. J. In *22nd International Symposium on Ballistics* Vancouver, BC, 2005; DEStech Publications: Lancaster, PA, 2005.
(6) Wetzel, E. D.; Lee, Y. S.; Egres, R. G.; Kirkwood, K. M.; Kirkwood, J. E.; Wagner, N. J. In *8th International Conference on Numerical Methods in Industrial Forming Processes*; Columbus, OH, 2004; American Institute of Physics: College Park, MD, 2004.
(7) Lee, B.-W.; Kim, I.-J.; Kim, C.-G. In *SEICO 09 SAMPE EUROPE 30th International Jubilee Conference Forum*; Paris, France, 2009; The Society for the Advancement of Material and Process Engineering: Covina, CA, 2009.
(8) Egres, R. G.; Lee, Y. S.; Kirkwood, J. E.; Kirkwood, K. M.; Wetzel, E. D.; Wagner, N. J. In *14th International Conference on Composite Materials*; San Diego, CA, 2003.
(9) Decker, M. J.; Halbach, C. J.; Nam, C. H.; Wagner, N. J.; Wetzel, E. D. *Compos. Sci. Technol.* **2007**, *67*, 565–578.
(10) Tan, V. B. C.; Tay, T. E.; Teo, W. K. *Int. J. Solids Struct.* **2005**, *42*, 1561–1576.
(11) Mahfuz, H.; Clements, F.; Rangari, V.; Dhanak, V.; Beamson, G. *J. Appl. Phys.* **2009**, *105*.
(12) Bazhenov, S. *J. Mater. Sci.* **1997**, *32*, 4167–4173.
(13) Lee, B. L.; Walsh, T. F.; Won, S. T.; Patts, H. M.; Song, J. W.; Mayer, A. H. *J. Compos. Mater.* **2001**, *35*, 1605–1633.
(14) Duan, Y.; Keefe, M.; Bogetti, T. A.; Cheeseman, B. A. *Int. J. Impact Eng.* **2005**, *31*, 996–1012.
(15) Duan, Y.; Keefe, M.; Bogetti, T. A.; Cheeseman, B. A. *Compos. Struct.* **2005**, *68*, 331–337.
(16) Duan, Y.; Keefe, M.; Bogetti, T. A.; Cheeseman, B. A.; Powers, B. *Int. J. Impact Eng.* **2006**, *32*, 1299–1312.
(17) Scott, B. R. In *18th International Symposium on Ballistics*; San Antonio, TX, 1999; pp 1184−1191; CRC Press: Danvers, MA, 1999.
(18) Zeng, X. S.; Tan, V. B. C.; Shim, V. P. W. *Int. J. Numer. Methods Eng.* **2006**, *66*, 1309–1330.

(19) Kirkwood, J. E.; Kirkwood, K. A.; Lee, Y. S.; Egres, R. G.; Wagner, N. J.; Wetzel, E. D. *Text. Res. J.* **2004**, *74*, 939–948.
(20) Kirkwood, K. M.; Kirkwood, J. E.; Lee, Y. S.; Egres, R. G.; Wagner, N. J.; Wetzel, E. D. *Text. Res. J.* **2004**, *74*, 920–928.
(21) Shockey, D. A.; Erlich, D. C.; Simons, J. W., Improved Barriers to Turbine Engine Fragments: Interim Report III, ImDOT/FAA/AR-99/8-III.
(22) Shockey, D. A.; Erlich, D. C.; Simons, J. W.; Shin, H.-S. Improved Barriers to Turbine Engine Fragments: Interim Report IV, DOT/FAA/AR-99/8-IV; Office of Aviation Research: Washington, DC, 2002.
(23) Kalman, D. P.; Wagner, N. J. *Rheol. Acta* **2009**, *48*, 897–908.
(24) Shim, S. E.; Kim, K.; Oh, S.; Choe, S. *Macromol. Res.* **2004**, *12*, 240–245.
(25) Kalman, D. P.; Wagner, N. J. *J. Rheol.* 2008.
(26) Lee, Y. S.; Wagner, N. J. *Ind. Eng. Chem. Res.* **2006**, *45*, 7015–7024.
(27) Egres, R. G.; Lee, Y. S.; Kirkwood, J. E.; Kirkwood, K. M.; Wetzel, E. D.; Wagner, N. J. In *14th International Conference on Composite Materials*; San Diego, CA, 2003.
(28) Lee, Y. S.; Wetzel, E. D.; Wagner, N. J. *J. Mater. Sci.* **2003**, *38*, 2825–2833.
(29) Stab resistance of personal body armor - National Institute of Justice Standard - NIJ0115.00, 2000.
(30) Bodt, B. A.; Tingey, H. B. *Nav. Res. Logist.* **1990**, *37*, 875–892.
(31) Cheeseman, B. A.; Bogetti, T. A. *Compos. Struct.* **2003**, *61*, 161–173.
(32) Bender, J. W.; Wagner, N. J. *J. Rheol.* **1996**, *5*, 899–916.
(33) Nam, C.; Decker, M. J.; Halbach, C. J.; Wetzel, E. D.; Wagner, N. J. In *SAMPE* Long Beach, CA, 2005; The Society for the Advancement of Material and Process Engineering: Covina, CA, 2009.
(34) Shenoy, S. S.; Wagner, N. J.; Bender, J. W. *Rheol. Acta* **2003**, *42*, 287–294.

AM900516W